



Open camera or QR reader and scan code to access this article and other resources online.

Phenotypic Correction of Murine Mucopolysaccharidosis Type II by Engraftment of *Ex Vivo* Lentiviral Vector-Transduced Hematopoietic Stem and Progenitor Cells

Miles C. Smith,¹ Lalitha R. Belur,¹ Andrea D. Karlen,¹ Olivia Erlanson,¹ Kelly M. Podetz-Pedersen,¹ Jessica McKenzie,² Jenn Detellis,² Khatuna Gagnidze,² Geoffrey Parsons,² Nicholas Robinson,² Shelby Labarre,² Saumil Shah,² Justin Furcich,³ Troy C. Lund,³ Hsing-Chen Tsai,² R. Scott Mclvor,^{1,*} and Melissa Bonner²

¹Center for Genome Engineering, Department of Genetics, Cell Biology and Development, University of Minnesota, Minneapolis, Minnesota, USA; ²bluebird bio, Inc., Cambridge, Massachusetts, USA; ³Department of Pediatrics, University of Minnesota, Minneapolis, Minnesota, USA.

Mucopolysaccharidosis type II (MPS II, Hunter syndrome) is an X-linked recessive lysosomal disease caused by deficiency of iduronate-2-sulfatase (IDS). The absence of IDS results in the accumulation of the glycosaminoglycans (GAGs) heparan sulfate and dermatan sulfate. Currently, the only approved treatment option for MPS II is enzyme replacement therapy (ERT), Elaprase. However, ERT is demanding for the patient and does not ameliorate neurological manifestations of the disease. Using an IDS-deficient mouse model that phenocopies the human disease, we evaluated hematopoietic stem and progenitor cells (HSPCs) transduced with a lentiviral vector (LVV) carrying a codon-optimized human IDS coding sequence regulated by a ubiquitous MNDU3 promoter (MNDU3-IDS). Mice treated with MNDU3-IDS LVV-transduced cells showed supraphysiological levels of IDS enzyme activity in plasma, peripheral blood mononuclear cells, and in most analyzed tissues. These enzyme levels were sufficient to normalize GAG storage in analyzed tissues. Importantly, IDS levels in the brains of MNDU3-IDS-engrafted animals were restored to 10–20% than that of wild-type mice, sufficient to normalize GAG content and prevent emergence of cognitive deficit as evaluated by neurobehavioral testing. These results demonstrate the potential effectiveness of *ex vivo* MNDU3-IDS LVV-transduced HSPCs for treatment of MPS II.

Keywords: lentiviral vector, mucopolysaccharidosis type II, iduronate-2-sulfatase, glycosaminoglycan, hematopoietic stem cell

INTRODUCTION

MUCOPOLYSACCHARIDOSIS TYPE II (MPS II, Hunter syndrome) is an X-linked recessive metabolic disorder caused by deficiency of the lysosomal hydrolase iduronate-2-sulfatase (IDS). Incidence of the disorder is ~1:160,000 male births.¹ Loss of IDS leads to disruption in the catabolism of the glycosaminoglycans (GAGs) heparan

sulfate and dermatan sulfate, which accumulate in lysosomes leading to progressive and multisystemic disease.² Manifestations include organomegaly, cardiopulmonary obstruction, skeletal dysplasias, and in the most severe cases, neurodegeneration and death by adolescence.³

The current standard of care for MPS II is enzyme replacement therapy (ERT), consisting of recombinant IDS

*Correspondence: Dr. R. Scott Mclvor, Department of Genetics, Cell Biology and Development, University of Minnesota, 6-160 Jackson Hall, 321 Church St. S.E., Minneapolis, MN 55455, USA. E-mail: mcivo001@umn.edu

© Miles C. Smith et al., 2022. Published by Mary Ann Liebert, Inc. This Open Access article is distributed under the terms of the Creative Commons Attribution Noncommercial License [CC-BY-NC] (<http://creativecommons.org/licenses/by-nc/4.0/>) which permits any noncommercial use, distribution, and reproduction in any medium, provided the original author(s) and the source are cited.

(Elaprase) infused intravenously.⁴ Patients on ERT show several improvements that correlate with reduced urine GAG levels, including reduced organomegaly and improved performance on the six-minute walk test.⁵ However, ERT fails to address some of the systemic disease burden. A 9-year follow-up of patients on ERT showed no improvements in pulmonary, ocular, skeletal, or central nervous system (CNS) manifestations,^{6,7} which has been attributed to low bioavailability of the enzyme in some tissues;⁷ for example, the administered enzyme does not cross the blood–brain barrier (BBB), leaving the neurological manifestations of the disease unaddressed.⁸ In addition, the treatment is expensive and requires weekly enzyme infusions.

Allogeneic hematopoietic stem cell transplantation (HSCT) has been considered a possible treatment for MPS II. Potential benefits of HSCT include a consistent level of enzyme for patients, avoiding the peaks and troughs common to periodic enzyme infusions, thereby replacing expensive and time-consuming weekly ERT infusions with the prospect of addressing CNS manifestations of the disease.^{7,9} However, HSCT is not a standard treatment for MPS II, as initial clinical testing met with poor outcomes due to low enzyme levels, graft versus host disease, sepsis, and patient death.¹⁰ Recent reports on HSCT for MPS II have shown some neurological benefits but also low levels of IDS activity and continued musculoskeletal problems.^{10,11} Thus, MPS II patients still have significant unmet need for a treatment that can address the limitations of ERT and allogeneic HSCT.

Successful gene therapy for lysosomal diseases relies on the production of bioavailable enzyme at a sufficient and consistent level both systemically and in the CNS that is not achieved by currently available treatment options. Bioavailable enzyme secreted from genetically modified cells containing the transgene would be available for metabolic cross-correction of unmodified cells by mannose-6-phosphate receptor-mediated endocytosis.¹² For MPS II, strategies have been developed that employ either adeno-associated virus (AAV) for *in vivo* IDS gene delivery to target tissues, such as the CNS, or lentiviral vector (LVV) for *ex vivo* IDS gene delivery to hematopoietic stem and progenitor cells (HSPCs).

CNS-directed AAV administration has shown effectiveness in transducing cells in the brain, leading to sustained IDS expression, GAG reduction, and improvement in neurobehavior.^{13–15} Systemic approaches have also shown improvement in neurobehavior.^{16,17} However, AAV-based approaches face several challenges including the invasiveness of direct CNS administration, pre-existing anti-AAV immune response, and scaling up to clinical doses.^{7,18,19}

Autologous, *ex vivo* LVV-based approaches look to improve upon allogeneic HSCT by providing higher levels of bioavailable systemic IDS, addressing CNS manifes-

tations, and reducing the possibility of graft versus host disease.^{9,19–21} In this study, we sought to develop a therapy that provides high and sustained levels of bioavailable IDS to address the systemic, including skeletal, and CNS manifestations of MPS II. Using an MPS II mouse model, we evaluated the efficacy of *ex vivo* LVV gene-modified HSPCs encoding a codon-optimized human IDS under the control of a constitutively active MNDU3 promoter (MNDU3-IDS) for treatment of MPS II.

MATERIALS AND METHODS

Animal husbandry

Animal care and procedures were compliant with and approved by the University of Minnesota Institutional Animal Care and Use Committee (IACUC). Animals were maintained at the University of Minnesota Research Animal Resources facilities under specific pathogen-free conditions. C57BL/6 iduronate-2-sulfatase knockout (IDS-KO) mice were graciously provided by Dr. Joseph Muenzer, and offspring were genotyped by polymerase chain reaction (PCR).²² These mice were backcrossed with C57BL/6 CD45.1 mice to generate IDS-KO animals on a congenic C57BL/6 CD45.1 background. Heterogeneity at CD45 was used for determination of donor chimerism in transplant recipients. Animals were fed food and water *ad libitum*.

MNDU3-IDS and MNDU3-GFP LVV production

Self-inactivating and replication-deficient third-generation MNDU3-IDS and MNDU3-GFP LVVs were produced by transient transfection of HEK293T cells. The transfection included several packaging plasmids encoding GAG/POL, REV, and VSV-G as well as a plasmid transfer vector. Purification of LVVs was carried out by chromatography and formulated before storage at less than or equal to -65°C .²³

Lentiviral transduction and transplant procedures

Whole bone marrow was harvested, red blood cells (RBCs) were lysed using ammonium chloride, and nucleated cells were enriched for the HSPC population by lineage depletion using Miltenyi Biotec's murine Direct Lineage Cell Depletion Kit as previously described.²⁴ For LVV transduction, lineage depleted cells were suspended in Dulbecco's modified Eagle medium (Gibco) with 10% fetal bovine serum (EquaFETAL; Atlas Biologicals) and supplemented with penicillin–streptomycin (10,000 U/mL), protamine sulfate (600 $\mu\text{g}/\text{mL}$), and stimulatory cytokines (mouse stem cell factor [mSCF, 50 ng/mL], mouse interleukin-3 [mIL-3, 20 ng/mL], and human interleukin-6 [hIL-6, 50 ng/mL]).

Lineage-depleted cells were transduced with either MNDU3-IDS or MNDU3-GFP LVV at a multiplicity of infection (MOI) of 50 and plated onto nontreated

suspension plates for 24 h at 37°C, 5% CO₂. One day before transplantation, MPS II male recipient animals 6–8 weeks of age were myeloablated by lethal irradiation at a dose of 900 cGy X-ray. Lethal irradiation was chosen as the method of myeloablation after busulfan treatment (25 mg/kg daily for 4 days) resulted in low levels of donor cell engraftment. Twenty-four hours later, transduced cells were harvested by centrifugation for 10 min, resuspended in phosphate-buffered saline (PBS), and then irradiated recipient mice were infused with 0.84–1.0 × 10⁶ cells via the lateral tail vein. Animals were observed daily for any clinical signs of declining health or unscheduled deaths, and blood and urine collections were done monthly.

Flow cytometry

Peripheral blood was collected from the submandibular vein into heparinized tubes, and the RBCs were lysed using RBC lysis buffer (No. 07850; Stem Cell Technologies). The leukocytes were stained with phycoerythrin (PE)-conjugated anti-murine CD45.1 and allophycocyanin (APC)-conjugated anti-murine CD45.2 (all antibodies from BioLegend) and then evaluated by flow cytometry using a BD Biosciences Canto cytometer. The data were analyzed using the FlowJo software (BD Biosciences), and donor cell engraftment was determined as the percentage of CD45.1⁺ or CD45.2⁺ cells present.

Vector copy number analysis in peripheral blood cells

The vector copy number (VCN), or number of vector copies present in diploid genomic DNA (gDNA), was assessed based on identification of the Psi-Gag sequence and normalization to a mouse house-keeping gene, *TERT*. Peripheral blood mononuclear cells (PBMCs) were isolated following RBC lysis using ACK Lysing Buffer (Cat. No. A1049201; Thermo Fisher), and gDNA was extracted using Qiagen DNA Extraction Kit (Cat. No. 51331), followed by quantitative polymerase chain reaction (qPCR) amplification of the Psi-Gag and mouse *TERT* (Cat. No. 4458369; Thermo Fisher) sequences.²⁵

Tissue processing

Animals were euthanized at 8 months of age by CO₂ asphyxiation and transcardially perfused with 50 mL of PBS. A necropsy was performed, and tissues (liver, spleen, kidney, brain, heart, lung, spinal cord, ileum, cecum, colon, eye, and bone marrow) were harvested, frozen on dry ice, and stored at –20°C until processed. A wide range of tissues was collected due to the multisystemic nature of MPS II, relevance to patient disease manifestations, and relevance to therapeutic approach. A portion of each tissue was fixed overnight in 10% neutral buffered formalin (VWR) at a ratio of 1:10–20 tissue to formalin and then after 24 h transferred to 70% ethanol for storage until paraffin embedding.

Tissues stored at –20°C were processed for biochemical analysis by homogenization in 0.9% saline using a Bullet Blender bead mill (Storm 24 Homogenizer; NEXT ADVANCE) as previously described¹⁵ and clarified by centrifugation in a 5424R Eppendorf centrifuge. The supernatants were termed tissue lysates and were used for protein, IDS, and GAG assays. After clarification, the tissue lysates were stored at –20°C until analyzed.

IDS enzyme assay

Plasma and tissue lysates were assayed for IDS activity in a fluorometric assay using 4-methylumbelliferyl α -L-iduronide 2-sulfate disodium salt (4-MU2S) as substrate (Cat. No. M334715; Toronto Research Chemicals) as previously described.⁹ 4-MU2S (5 mg) substrate was dissolved in 8.33 mL distilled water to yield a 1.25 mM working solution. Twenty microliters aliquots of working substrate were mixed with 10 μ L aliquots of plasma or tissue lysates and incubated at 37°C for 1.5 h. Then, 20 μ L of PiCi Buffer (0.2 M Na₂HPO₄ + 0.1 M citric acid, 0.02% sodium azide, pH 4.5) was added to stop the IDS reaction. Ten microliters of 5 μ g/mL alpha-L-iduronidase (IDUA; Cat. No. 4119-GH; Bio-Techne) was added and the mixture was incubated at 37°C overnight.

The reaction was terminated by the addition of 200 μ L stop buffer (0.5 M Na₂CO₃ + 0.5 M NaHCO₃, pH 10.7). Tubes were then centrifuged at ~13,000 rpm for 1 min. Supernatant was transferred into a black 96-well round bottom plate, and the resulting fluorescence was measured using a Bio-Tek Synergy Mx plate reader with excitation at 355 nm and emission at 460 nm. IDS catalyzes the reaction of 4-MU2S into nonfluorescent 4-methylumbelliferone (4-MU) iduronide, and then IDUA catalyzes cleavage of the nonfluorescent 4-MU iduronide into fluorescent product 4-MU. A 4-MU (No. M1381; Sigma) standard curve was used for the calculation of 4-MU generated in the reaction. Protein was measured using the Pierce protein assay reagent (Cat. No. 22660; Thermo Fisher). Enzyme activity is expressed as nmol 4-MU released per mg protein per hour (nmol/h/mg) for tissues extracts, and as nmol/h/mL for plasma. All samples were assayed in duplicate.

GAG assay

Tissue lysates were incubated with proteinase K (20 mg/mL) at a ratio of 1:10 (ProK:tissue lysate) at 55°C overnight, followed by heat inactivation of the proteinase K by boiling for 10 min. Tissue lysates were further digested with 200 units of DNase and 2 mg of RNase per 50 μ L tissue lysate at room temperature overnight with gentle mixing. DNase and RNase were heat inactivated by boiling for 10 min. GAG levels were then determined using the Blyscan Sulfated GAG Assay Kit (Biocolor Life Science Assays, Cat. No. CLRB1000; Accurate Chemical, NY, Inc.) according to the manufacturer's protocol. For tissue GAGs, protein was measured using the Pierce

protein assay (Cat. No. 22660; Thermo Fisher) and results were expressed as μg GAG/mg protein. For urine, GAG levels were also assessed using the Blyscan assay, normalizing to urine creatinine levels and expressed as μg GAG/mg creatinine. Creatinine levels were determined using a creatinine assay kit (MAK080; Sigma).

Histology

For Alcian blue staining of GAGs, formalin-fixed paraffin-embedded (FFPE) tissues were deparaffinized, rehydrated, and then exposed to 1% Alcian blue in 3% acetic acid. Tissues were rinsed with distilled water and counterstained with 0.1% Nuclear Fast Red Kernechtrot. The tissues were then dehydrated and mounted. Semiquantitative Alcian blue staining was scored as previously described.²⁶

For immunohistochemistry of lysosomal associated membrane protein-1 (LAMP-1), dry FFPE slides were loaded onto a Leica BOND Rx instrument and baked at 60°C, placed in BOND Dewax Solution (No. AR9222; Leica) at 72°C, rinsed with ethanol, and rinsed in BOND Wash Solution 10× Concentrate (No. AR9590; Leica). Slides were then pretreated with HIER Solution, BOND Epitope Retrieval Solution 2 and 1 (No. AR9961; Leica), before being washed with BOND Wash Solution.

Slides were then blocked and stained using a peroxidase block, Rodent Block “M” (No. RBM961L; Biocare Medical), Primary LAMP-1 at a final concentration of 0.25 $\mu\text{g}/\text{mL}$ (No. MCA497G; Bio-Rad), Rat Probe (No. RTP629L; Biocare Medical), Rat Polymer (No. RTH630L; Biocare Medical), Mixed DAB Refine (No. DS9800; Leica), and hematoxylin, with BOND Wash Solution used between each. Finally, slides were mounted after dehydration with ethanol and xylene. LAMP-1 scoring was based on the average percentage of LAMP-1-positive cells and their average intensity for each location. Scoring was calculated by multiplying the proportion of stained cells by the intensity of staining.

In situ hybridization (ISH) was performed using RNAscope[®] 2.5 LS Probe-BBB-Lenti-G-sense (Cat. No. 519048; ACD) to identify the LVV provirus integrated into gDNA. The tissues were stained on a Leica BOND Rx robot using ACD RNAscope 2.5 LSx Reagent kit—RED (Cat. No. 322750; ACD) according to the manufacturer’s instructions. A mouse Brain Slicer Matrix (Brain Matrice Stainless Steel, mouse, coronal, 1 mm cut, Cat. No. 69-2175-1; AgnThos, Lidingö, Sweden) was used to section the brains into six coronal slices, and images were scored based on the number of dots per cell and number of positive cells per 200× field.

Radiography and image analysis

One week before mouse euthanasia, experimental mice were sedated with 5% isoflurane, and whole-body X-ray or Micro-computed tomography (Micro-CT) images were acquired using a Bruker Xtreme or Siemens Inveon PET/CT machine, respectively. The acquired DICOM files

were exported from the machines and converted to Imaris image files using the Imaris File Converter software. This conversion resulted in an X-ray or Micro-CT file that could be analyzed using the Imaris 3D Analysis software. Imaris 3D Analysis software was then utilized to obtain body measurements of the X-ray or Micro-CT scans, including zygomatic arch diameter.

Barnes maze

The Barnes maze is a measure of spatial navigation and memory.²⁷ It consists of a circular platform with 20 holes positioned around the periphery, all of which are blocked except for 1 hole, which has an escape box positioned underneath that the mouse can access using an inclined ramp. Visual cues are placed on the walls around the maze for spatial navigation. The animal is released into the center of the maze with the lights dimmed, bright overhead lights are then turned on, and the mouse is given 3 min to explore the maze. If the mouse does not enter the escape box within 3 min, it is guided to the escape hole and left there for 30 s before returning to its home cage. The mice were trained on the Barnes maze for 4 days at four trials a day, with an interval of 12–15 min between any two consecutive trials for each animal. The time taken by the animal to escape was recorded as latency to escape.

Fear conditioning

This associative learning task assesses a fear response (*i.e.*, time spent freezing) to a conditioned stimulus (cue) that is predictive of an unconditioned stimulus (mild foot shock) introduced during training trials.²⁸ Data collection and analysis were semi-automated via video-monitoring (Med Associates, Inc.). On the conditioning day (training day; day 1), the test chamber was sprayed with a solution of Simple Green as an olfactory cue, and mice were exposed to a series (five pairings; 1-min intertrial interval) of cue (80 dB white noise tone and light) presentations (15 s in duration) that co-terminated with a mild foot shock (0.7 mA, 1 s in duration). Twenty-four hours later, a cued fear test was performed in a test chamber with altered contextual elements (floor, wall, and odor) and consisted of three 1-min baseline (nonspecific freezing behavior) and three 1-min light and sound cue exposure (cued fear) periods. Freezing response was assessed during both the baseline and cue testing sessions. Percent difference in freezing during the cued fear test was taken as:

$$\left(\frac{\text{Average freezing during cue} - \text{average freezing in baseline}}{\text{average freezing in baseline}} \right) \times 100.$$

Statistics

GraphPad Prism was used for all graphing and statistics. Error bars on graphs represent group mean \pm standard deviation. Multiple group comparisons were evaluated by

one-way or two-way analysis of variance (ANOVA) for IDS activity, urine and tissue GAGs, and Barnes maze. Fear conditioning data were analyzed by nonparametric comparisons using the Mann–Whitney *U* test. Histological data were analyzed by one-way ANOVA and Tukey's multiple comparisons test. *p* Values of <0.05 were considered statistically significant for all tests. Radiographic data were grouped into mouse treatment types and evaluated using the Student's *t*-test.

RESULTS

Ex vivo LVV gene therapy study design

To test the potential of MNDU3-IDS LVV-transduced HSPCs in treating MPS II, donor HSPCs from MPS II KO mice (IDS^{Y/-}) were transduced *ex vivo* with an LVV carrying a codon-optimized IDS encoding gene regulated by a constitutive MNDU3 promoter (Fig. 1A). This MNDU3-IDS group was compared with three control groups: (1) MNDU3-GFP LVV-transduced group (affected control),

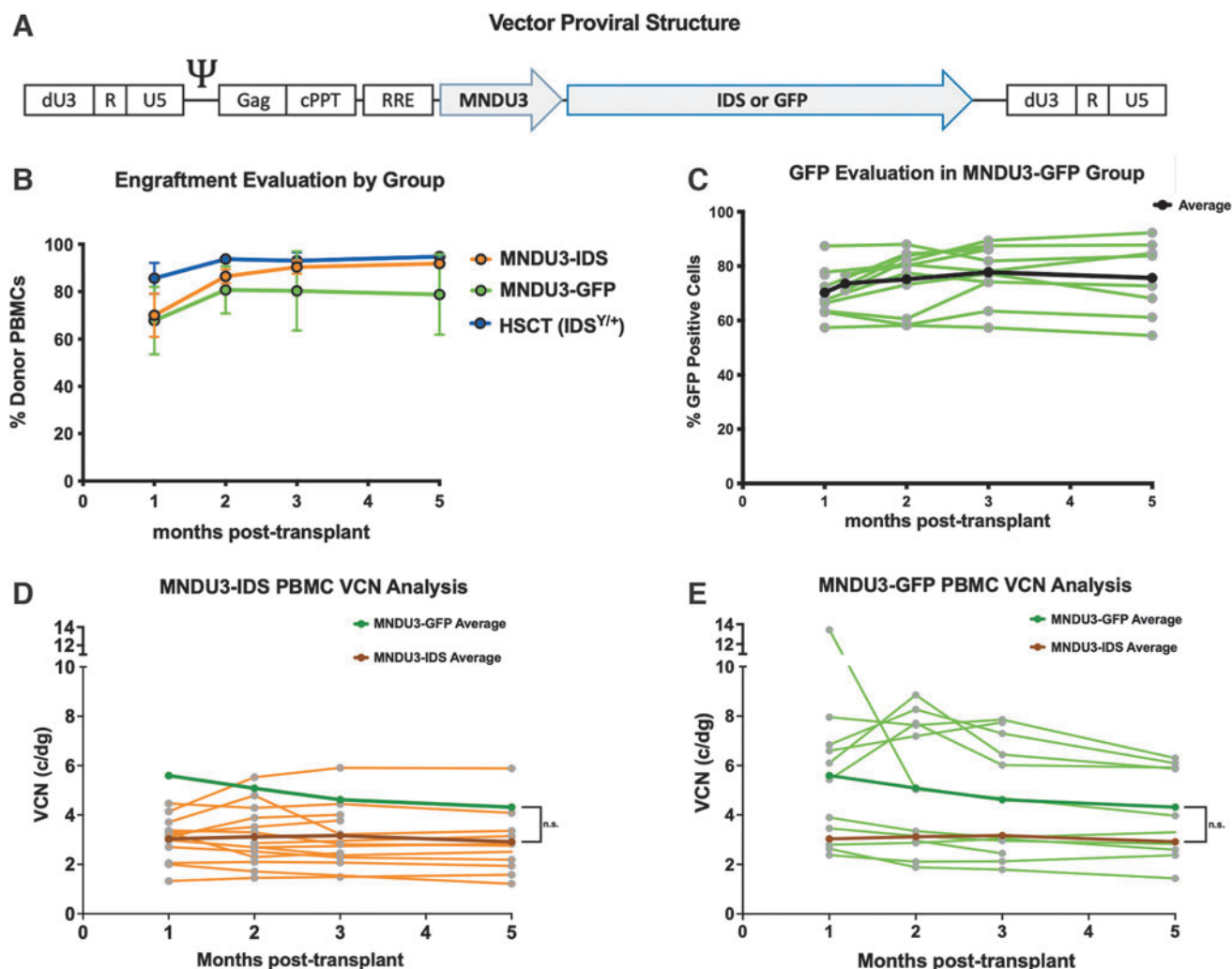


Figure 1. Donor chimerism and VCN analysis in transplant recipients. **(A)** Diagram of the LVV proviral construct containing a codon-optimized IDS or GFP sequence regulated by the MNDU3 promoter. MNDU3—myeloproliferative sarcoma virus U3 region with negative control elements deleted and dl587rev primer binding site added,⁴³ IDS—codon-optimized human IDS. **(B)** Mean donor engraftment for the three transplant groups as indicated in the key. **(C)** Percentage of GFP-positive cells for each animal in the MNDU3-GFP group. *Green lines* show individuals, whereas the *black line* indicates GFP+ average over time. In **(D, E)**, PBMCs were analyzed by qPCR to determine VCN per cell (c/dg) post-transplant. The *dark orange* and *dark green lines* on each graph represent the MNDU3-IDS and MNDU3-GFP average VCNs by month, respectively. **(D)** MNDU3-IDS LVV transplant group VCN evaluation. *Orange lines* show individual animal VCN by month. **(E)** MNDU3-GFP LVV transplant group, VCN evaluation. *Green lines* show individual animals VCN by month. Some time points were not collected due to COVID-19 lockdown. (For donor chimerism data, this includes two month 2, two month 3, and four month 5 MNDU3-IDS samples; one month 2, one month 3, and three month 5 MNDU3-GFP samples; and one month 2, one month 3, and one month 5 HSCT samples. For VCN, this includes two month 3 and two month 5 MNDU3-IDS samples, and one month 3 and two month 5 MNDU3-GFP samples.) Sample size for group engraftment: MNDU3-IDS *N* = 9–14, MNDU3-GFP *N* = 8–12, HSCT *N* = 10–11. Sample size for GFP evaluation: MNDU3-GFP *N* = 12. Sample size for VCN analysis: MNDU3-IDS *N* = 14 and MNDU3-GFP *N* = 12. Error bars show mean ± SD for **(B–E)**. Ψ, packaging signal; cPPT, central polypurine tract; dU3, deleted U3 region (self-inactivating); Gag, group-specific antigen sequence; HSCT, hematopoietic stem cell transplantation; IDS, iduronate-2-sulfatase; LVV, lentiviral vector; PBMCs, peripheral blood mononuclear cells; qPCR, quantitative polymerase chain reaction; R, repeat region; RRE, rev response element; SD, standard deviation; U5, unique 5' region; VCN, vector copy number.

(2) a group transplanted with wild-type IDS^{Y/+} bone marrow from congenic C57BL/6 littermates (HSCT control), and (3) an untreated wild-type group (unaffected control). For the MNDU3-IDS and MNDU3-GFP transplantation groups, lineage-depleted IDS^{Y/-} bone marrow was transduced overnight with either the MNDU3-IDS or MNDU3-GFP LVV at an MOI of 50.

For the HSCT group, IDS^{Y/+} HSPCs were similarly harvested and enriched and then transplanted without transduction or *ex vivo* culture. Donor HSPCs were injected into 6- to 8-week-old myeloablated (900 cGy X-ray) IDS^{Y/-} C57BL/6 mice at a dose of $0.84\text{--}1.0 \times 10^6$ cells/mouse. Mice at 6 to 8 weeks of age are presymptomatic and have been used in past studies to evaluate the prevention of skeletal and neurobehavioral manifestations.^{15,19,20}

Peripheral blood and urine were collected every month (except for month 4 post-transplant when the mice underwent neurobehavioral testing) to evaluate donor cell engraftment, IDS enzyme activity in both the plasma and PBMCs, VCN in PBMCs, and urine GAG excretion. At 4 months post-transplant, the mice underwent neurobehavioral evaluation consisting of Barnes maze and fear conditioning. Approximately 1 week after neurobehavior testing, the mice underwent full-body skeletal analysis by X-ray or Micro-CT imaging. At 5 months post-transplant, the animals were euthanized, perfused, and necropsied. Tissue samples were collected for measuring the IDS enzyme activity and GAG accumulation, as well as histological evaluation. Tissues assayed included the liver, spleen, kidney, heart, lung, brain, spinal cord, eye, ileum, cecum, colon, and bone marrow.

Donor chimerism in transplant recipients

Donor cell engraftment versus recipient cell repopulation post-transplant was evaluated by distinction of CD45.1 versus CD45.2 via flow cytometry. All three transplant groups showed high levels (>60%) of engraftment at 1-month post-transplant (Fig. 1B). In the following months, engraftment increased 10–20% and then stabilized in all three transplant groups. By 5 months post-transplant, MNDU3-IDS and HSCT groups showed engraftment of >90%, whereas the MNDU3-GFP group showed engraftment of ~80%. PBMCs from MNDU3-GFP treated animals were on average 75% GFP positive, comparable to the level of engraftment shown by CD45 donor chimerism analysis (Fig. 1C). Overall, these analyses revealed high levels of stable donor cell engraftment in all three transplant groups, and specifically in the MNDU3-GFP group, stable engraftment of gene-modified cells, as assessed by GFP+ PBMCs.

VCN analysis in PBMCs

VCN in PBMCs of MDU3-IDS and MND-GFP transplanted groups was determined by qPCR throughout the 5-month time course of the experiment. The MNDU3-IDS

group had PBMC VCN between 1 and 6 c/dg and the MNDU3-GFP group had similar values of 2–8 c/dg during in-life collections (Fig. 1D, E). One animal in the MNDU3-GFP group initially had PBMC VCN of 13 c/dg at 1-month post-transplant, but VCN decreased to 4 c/dg by 5 months post-transplant (Fig. 1E). Throughout the study period, the average VCN in the MNDU3-GFP group trended higher compared with the MNDU3-IDS group (thick green and orange lines shown in Fig. 1D, E), but this difference was not statistically significant ($p=0.1320$). Taken together with the donor chimerism results, groups receiving gene-modified HSPCs exhibited stable engraftment of gene-modified cells.

Peripheral blood IDS enzyme activity and urine GAG excretion

Expression of the MNDU3-IDS transgene was assessed by IDS enzyme activity assay both in the peripheral blood plasma and in PBMCs. The following in-life means are a combined post-transplant average of all samples collected monthly by group. Wild-type mice had a mean of 30.5 nmol/h/mL IDS in the plasma (Fig. 2A) and 31.5 nmol/h/mg protein in PBMCs (Fig. 2B). The MNDU3-GFP group showed no detectable activity above background in the plasma and low-level background activity in PBMCs. Remarkably, MNDU3-IDS-treated animals had an average of 8.2×10^3 nmol/h/mL IDS activity in plasma, 269 times higher than the wild-type level of activity ($p<0.01\text{--}0.0001$) and a mean of 5.7×10^3 nmol/h/mg protein in PBMCs, 180 times the wild-type level of activity ($p<0.01\text{--}0.001$).

MPS II mice engrafted with wild-type HSPCs (HSCT group) had a mean of 4 nmol/h/mL IDS in plasma and a mean of 15 nmol/h/mg protein in PBMC extracts, both below wild-type levels, although this was statistically significant only for plasma IDS ($p<0.001$). These IDS enzyme activity levels were maintained from 1-month post-transplant to the end of study at 5 months post-transplant. In summary, supraphysiological levels of IDS enzyme activity were seen in both plasma and PBMCs in the MNDU3-IDS transplant group.

Before treatment, all the groups showed elevated levels of urine GAG excretion (~2,900 μg GAG/mg creatinine) when compared with wild-type mice (~600 μg GAG/mg creatinine) and were not significantly different from one another. After transplant, the MNDU3-GFP group maintained a high level of ~3,000 μg GAG/mg creatinine for the duration of the study, which was significantly higher compared with all other groups throughout the remainder of the study ($p<0.05\text{--}0.001$) (Fig. 2C). In contrast, the MNDU3-IDS and HSCT groups showed normalization of excreted GAGs that was not significantly different from wild type. The reduction in excreted GAGs was maintained throughout the study for both the MNDU3-IDS and HSCT groups.

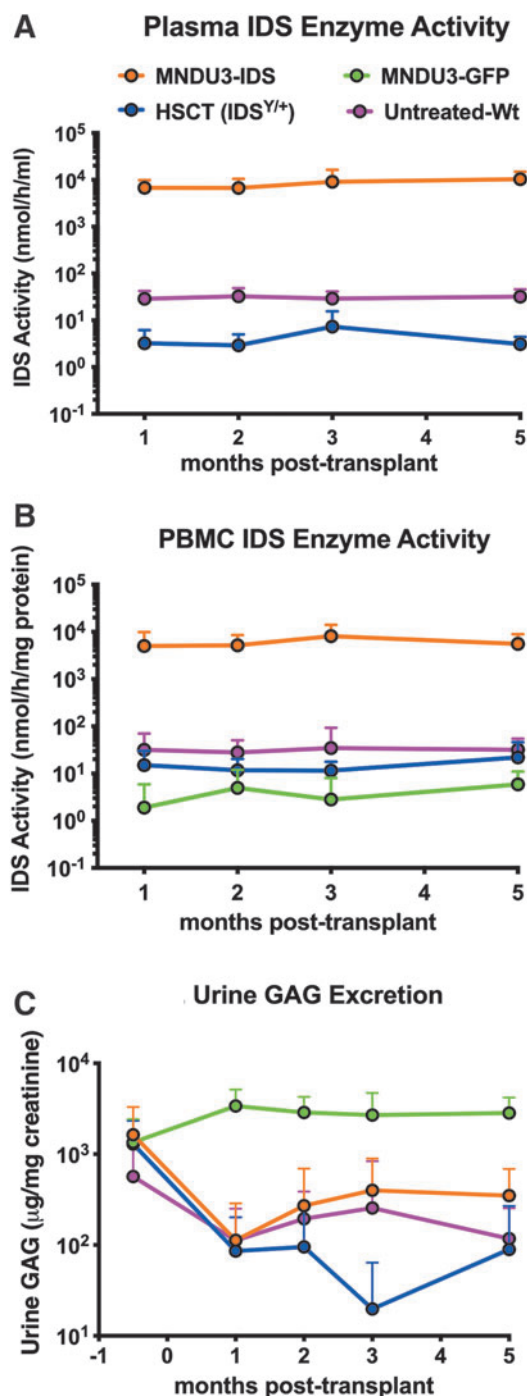


Figure 2. Plasma IDS, PBMC IDS, and urine GAG excretion. **(A, B)** Plasma and PBMC mean IDS enzyme activities by month for each group indicated in the key. All MNDU3-GFP plasma samples have been omitted, as the activity measured was below LOQ. **(C)** The mean excreted GAGs in urine collected 2 weeks before the study and then monthly thereafter for the groups indicated in the key. Some time points were not collected due to COVID-19 lockdown (for plasma, PBMC, and urine GAGs; two month 3 and two month 5 MNDU3-IDS samples, one month 3 and two month 5 MNDU3-GFP samples, and two month 3 and two month 5 Untreated-Wt samples). Sample size for IDS activity assays: MNDU3-IDS $N=11-14$, MNDU3-GFP $N=9-12$, HSCT $N=10$, and Untreated-Wt $N=9-12$. Sample size for Urine GAG assays: MNDU3-IDS $N=4-9$, MNDU3-GFP $N=6-10$, HSCT $N=1-9$, and Untreated-Wt $N=1-5$. Error bars show mean \pm SD. GAG, glycosaminoglycan; LOQ, limit of quantification; Wt, wild type.

Tissue IDS enzyme activity and GAG normalization in MNDU3-IDS-treated mice

The potential for IDS cross-correction was evaluated by assaying for enzyme activity in nonhematopoietic peripheral and CNS tissues collected at the end of study 5 months post-transplant. Wild-type mice showed varying levels of IDS activity by tissue, ranging from a mean of 15 nmol/h/mg protein in the heart to 278 nmol/h/mg protein in the brain (Fig. 3A). The MNDU3-GFP group showed little to no IDS activity in any peripheral or CNS tissues. MNDU3-IDS-treated mice had IDS activities that far exceeded those of normal unaffected controls in peripheral tissues and were significantly greater than those of MNDU3-GFP-treated mice.

Tissues with resident hematopoietic cells showed the highest IDS levels, with a 140-fold increase over wild-type levels in the liver ($p < 0.0001$) and a 52-fold increase over wild-type levels in the spleen ($p < 0.0001$). Cross-correction of nonhematopoietic tissues was also observed; there was a 14-fold increase in the IDS enzyme activity over wild-type levels in the kidney ($p < 0.05$) and an 18-fold increase over wild-type levels in the heart ($p < 0.0001$) (Fig. 3A). In contrast, MPS II animals engrafted with wild-type HSPCs generally showed IDS enzyme activity levels lower than wild-type levels in the liver ($p < 0.001$), spleen ($p < 0.001$), kidney ($p < 0.05$), and lung ($p < 0.01$), but not heart ($p = 0.179$).

A key goal of potential therapeutics for MPS II is achieving high levels of IDS in the CNS to address neurological manifestations of the disease. Consistent with previous reports,^{15,19} in wild-type mice, we observed a high level of IDS enzyme activity in the brain at an average of 278 nmol/h/mg. Animals engrafted with MNDU3-IDS-transduced HSPCs had a mean of 35.6 nmol/h/mg IDS activity in brain tissue, $\sim 13\%$ that of wild type on average ($p < 0.01$) (Fig. 3A), and this level of IDS activity was sufficient to normalize GAG accumulation in the CNS (Fig. 3B). In the spinal cord, MNDU3-IDS-treated mice exhibited physiological levels of IDS activity (162.6 nmol/h/mg). MPS II animals engrafted with wild-type HSPCs had $< 1\%$ of wild-type IDS activity in the brain ($p < 0.01$). In the spinal cord, the HSCT group showed only 3% of wild-type IDS activity (4.5 nmol/h/mg; $p < 0.0001$).

Collected tissues were analyzed for GAG accumulation. In the MNDU3-GFP affected control group, levels of GAG were consistently higher than wild-type animals in all organs; the liver, kidney, and spleen in the MNDU3-GFP group had $36\times$ ($p < 0.0001$), $36\times$ ($p < 0.0001$), and $16\times$ ($p < 0.05$) significantly increased GAG compared with wild-type animals, respectively. In CNS tissues, MNDU3-GFP mice exhibited GAG levels $2.3\times$ higher in the brain ($p < 0.001$) and $9.7\times$ higher in the spinal cord ($p < 0.0001$) compared with wild-type controls. In contrast, the MNDU3-IDS group showed normalization of

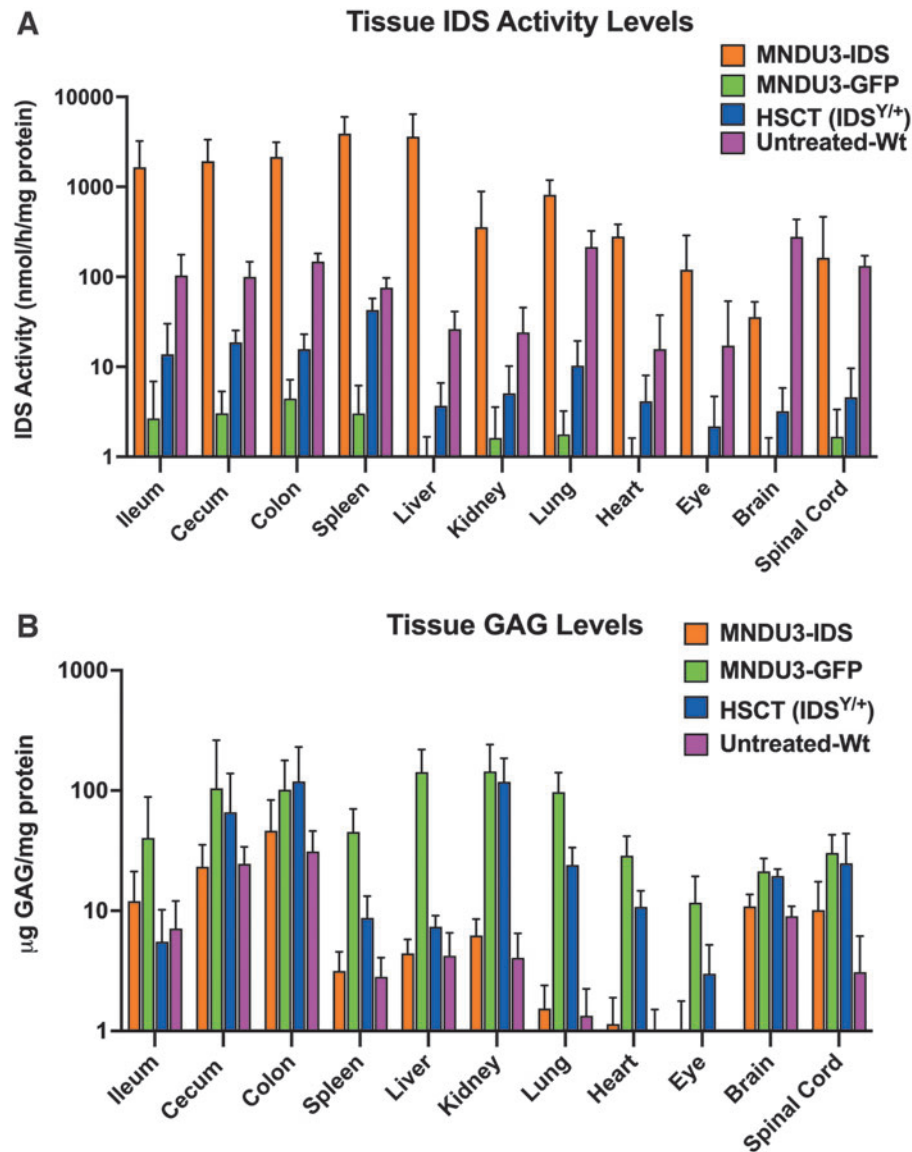


Figure 3. Tissue IDS enzyme and GAG levels. **(A)** The mean IDS activity in each indicated tissue for each experimental group shown in the key. **(B)** The mean GAG levels in the indicated tissue and for animal groups shown in the key. Sample size for IDS activity and GAG assays: MNDU3-IDS $N=9-12$, MNDU3-GFP $N=8-11$, HSCT $N=7-10$, and Untreated-Wt $N=8-11$. Error bars show mean \pm SD.

GAG levels in all peripheral tissues analyzed. In the CNS, GAG levels were normalized in the brain and not significantly different from wild-type levels ($p=0.1214$) (Fig. 3B). Interestingly, the spinal cord in MNDU3-IDS transplanted animals had significantly higher GAG accumulation than wild-type mice ($p<0.05$), even though wild-type levels of IDS were observed (Fig. 3A, B).

However, GAG accumulation was nonetheless reduced when compared with the affected ($p<0.001$) or HSCT control groups ($p<0.05$). For the HSCT group, GAG levels were higher than wild type in all tissues ($p<0.01$ to $p<0.001$) except the ileum. There was major improvement in hemopoietic resident tissues such as the liver and spleen, but complete GAG normalization was not ob-

served. Finally, HSCT mice showed no reduction of storage material in the brain or spinal cord, which were not significantly different from affected controls. MNDU3-IDS LVV-transduced HSPC transplanted recipients with significantly increased tissue IDS enzyme activity thus exhibited concomitant reduction in tissue GAG accumulation, including in the CNS.

Histological analysis

GAG content in the liver, kidney, bone marrow, and spleen was additionally evaluated by Alcian blue staining. Large amounts of GAG accumulated in the bone marrow and the spleen in the MNDU3-GFP control group, with resident macrophages contributing to the majority of GAG

accumulation in these tissues. Staining in the MNDU3-IDS and HSCT groups revealed a substantial reduction in GAG content compared with the MNDU3-GFP group (Fig. 4C, G and Supplementary Fig. S1A, D). In MNDU3-GFP mice, GAG content in the liver was mainly located in the cytoplasm of hepatocytes, leading to large amounts of cytoplasmic vacuolization.

The HSCT group showed a reduction of GAG content in the liver but retained a small amount of storage material in the perivascular region. GAG levels in the liver and kidney of the MNDU3-GFP group were significantly higher than that of the MNDU3-IDS group ($p < 0.0001$), which was normalized to wild-type levels. In the kidney, GAG content of the HSCT group was not significantly

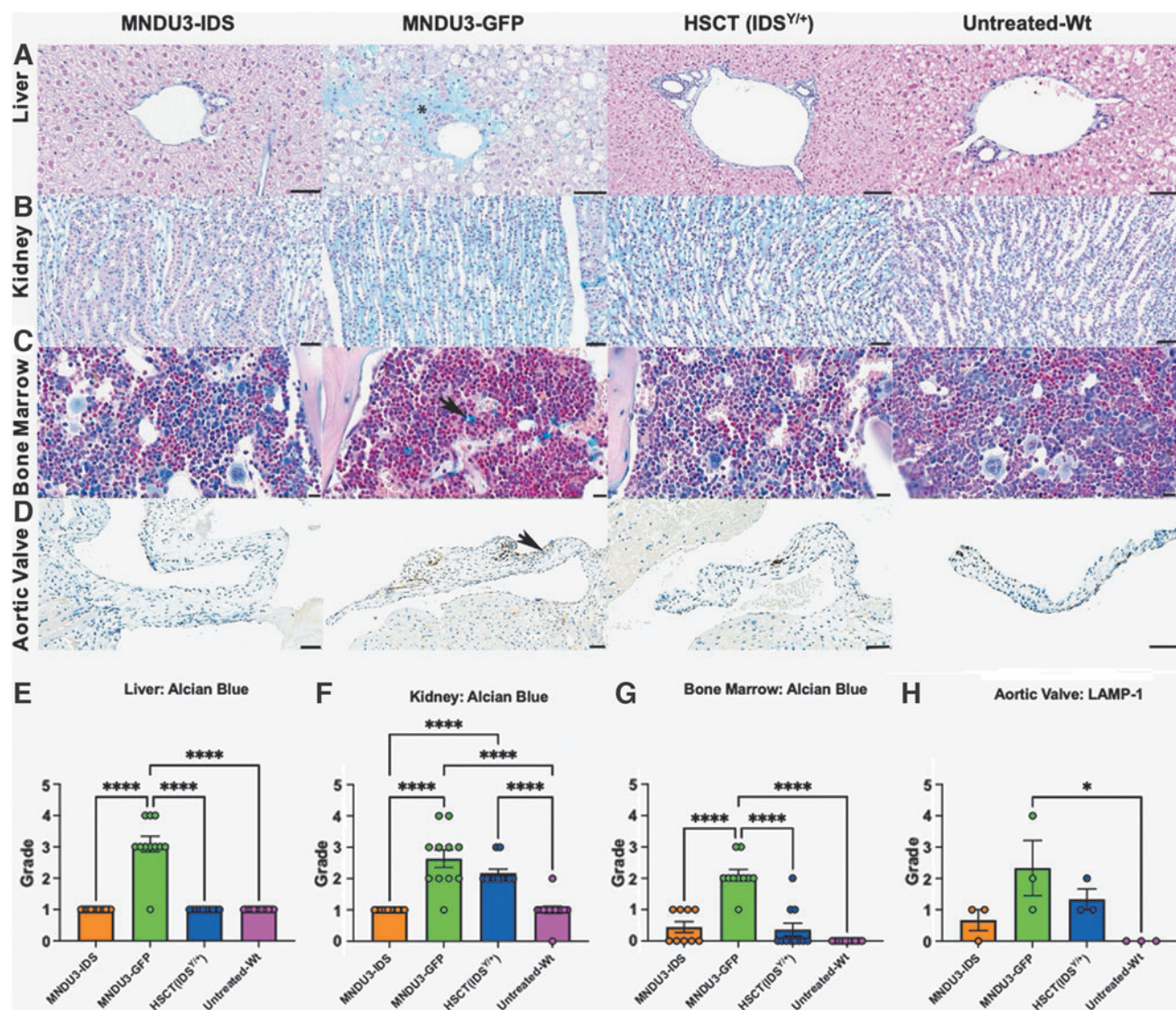


Figure 4. Histological evaluation. Micrographs are presented by group, left to right: MNDU3-IDS, MNDU3-GFP, HSCT, and Untreated-Wt. **(A)** Liver, AB staining. The MNDU3-IDS and Untreated-Wt groups are AB negative. The MNDU3-GFP group has extensive deposition of AB-positive material in the perivascular region extending out into the acini disrupting the architecture (*asterisk*). There is extensive vacuolization of the hepatocytes with variable amounts of cytoplasmic AB-positive material in hepatocytes. The HSCT shows a small amount of AB-positive material in the perivascular regions. Scale bars = 50 μ m. **(B)** Kidney, AB staining. The MNDU3-IDS and Untreated-Wt groups have a normal amount of AB-positive material. The MNDU3-GFP and HSCT groups have AB-positive material within the collecting duct epithelial cell cytoplasm. Scale bars = 50 μ m. **(C)** Bone marrow, AB staining. The MNDU3-IDS, HSCT and Untreated-Wt groups are AB negative. The MNDU3-GFP group has numerous macrophages with abundant cytoplasmic AB-positive material (*black arrow*). Scale bar = 10 μ m. **(D)** Aortic valve, LAMP-1 IHC. The MNDU3-IDS group has scant LAMP-1 positivity within the valvular stroma. The MNDU3-GFP group has extensive LAMP-1 positivity throughout the valvular stroma (*black arrow*). The HSCT group has a small amount of LAMP-1 positivity throughout the valvular stroma. The Untreated-Wt group is LAMP-1 negative. Scale bar = 50 μ m. Semiquantitative scoring of AB staining in the **(E)** liver, **(F)** kidney, and **(G)** bone marrow. **(H)** LAMP-1 IHC quantitative scoring of the aortic valve. Error bars show SEM. Statistics done by one-way ANOVA. * $p < 0.05$, **** $p < 0.0001$. AB, Alcian blue; ANOVA, analysis of variance; IHC, immunohistochemistry; LAMP-1, lysosomal associated membrane protein-1; SEM, standard error of the mean.

different from the MNDU3-GFP group but scored significantly different from the MNDU3-IDS and wild-type groups. Accumulation in the kidney was largely in the interstitium and glomeruli (Fig. 4A, B, E, F).

LAMP-1 is upregulated in cells with persistent GAG accumulation, such as IDS-deficient cells. Therefore, LAMP-1 can be used as a marker for cellular damage.²⁹ The MNDU3-GFP group showed significantly higher levels of LAMP-1 in the myocardium and aortic valve compared with wild-type mice ($p < 0.05$). The MNDU3-IDS group showed normalized LAMP-1 staining in the myocardium. In the aortic valve, however, there was a reduction in LAMP-1 staining, but this was not significantly different when compared with the MNDU3-GFP group. In the myocardium, the HSCT group was not significantly different from wild type but did show low levels of LAMP-1 positivity in the aortic valve (Fig. 4D, H and Supplementary Fig. S1B, E).

LAMP-1-positive macrophages were detected only in the colons of the MNDU3-GFP group (Supplementary Fig. S1C, F). Taken together with the GAG assay results, this histological analysis shows that MNDU3-IDS can effectively reduce storage material to or near wild-type levels in the tissues analyzed, with the exception of the aortic valve and spinal cord.

LVV transduction was detected by ISH for both the MNDU3-IDS and MNDU3-GFP groups. LVV-positive cells were seen in the spleen and bone marrow, but not in the liver (Supplementary Fig. S2C, D). In the brain, LVV-positive cells were seen in the meninges, as well as the

perivascular regions (Supplementary Fig. S2A, B, D), supporting a mechanism of gene-modified hematopoietic cell engraftment in the CNS. Additionally, ISH was employed to evaluate two multicentric lymphomas that occurred in two mice from the MNDU3-IDS group. LVV ISH performed on the spleen and liver was negative in the neoplastic lymphocytes. Thus, the two instances of lymphoma were considered spontaneous and unrelated to the vector.

Skeletal analysis

This MPS II mouse model exhibits a skull enlargement phenotype, which includes an increase in the cross-sectional area of the zygomatic bones.²² To assess the impact of this therapy on skeletal manifestations, mice were imaged by either full body X-ray or Micro-CT to evaluate zygomatic arch thickening at 4 months post-transplant. An additional control group of untreated MPS II IDS^{Y/-} mice ($n = 8$) was also imaged. Figure 5A shows representative microradiographs from all five groups, with arrows indicating the location of the zygomatic arch. In these images, thickness of the zygomatic arch was measured as the diameter of the bone at this location.

MNDU3-IDS and HSCT groups showed thickness similar to that of normal wild-type mice. However, mice from the MNDU3-GFP or untreated MPS II mice had significantly more bone thickening than untreated wild-type mice ($p < 0.01$, $p < 0.0001$) (Fig. 5B). MNDU3-GFP-treated mice showed significantly thicker zygomatic bones compared with the MNDU3-IDS-treated mice ($p < 0.05$), although not to the same extent as untreated MPS II

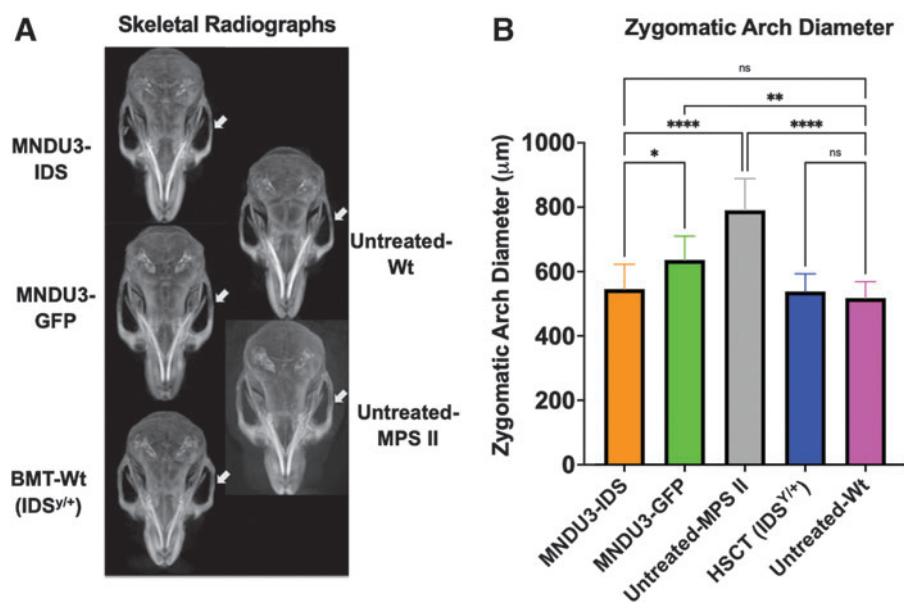


Figure 5. Skeletal analysis. **(A)** Example radiographs of mouse skulls obtained by Micro-CT analysis for the indicated experimental group. Arrows indicate zygomatic arch location. **(B)** Comparison of zygomatic arch diameter by group. Significance was determined by one-way ANOVA with Tukey's multiple comparisons test. Sample sizes: MNDU3-IDS $N = 13$, MNDU3-GFP $N = 11$, Untreated-MPS II $N = 8$, HSCT $N = 10$, and Untreated-Wt $N = 11$. Error bars show SEM. * $p < 0.05$, ** $p < 0.01$, **** $p < 0.0001$. Micro-CT, micro-computed tomography; MPS II, mucopolysaccharidosis type II; ns, no significance.

controls ($p < 0.0001$). These data thus reveal a trend toward normalization of the zygomatic arch skeletal defect in MNDU3-IDS as well as HSCT mice.

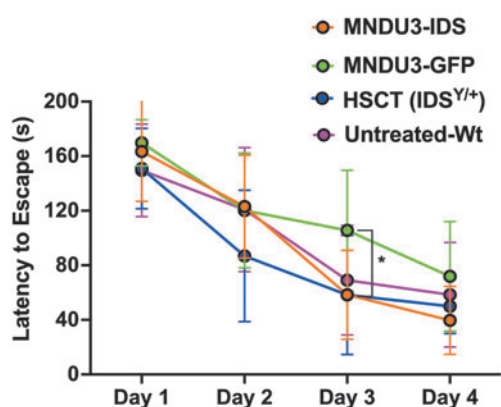
Neurobehavioral analysis

At 4 months post-transplant (6 months of age), mice from all the four groups underwent neurobehavioral testing to assess neurocognitive function. A 20-hole Barnes maze was used as a test of spatial navigation and memory and consisted of four 3-min trials a day for 4 days. On day 1, all groups scored ~ 180 s latency to escape. On day 3, the MNDU3-GFP group performed worse than the wild-type

group ($p < 0.05$), demonstrating a latency to escape of 105 s compared with 69 s. In contrast, the MNDU3-IDS and HSCT groups performed similarly to the wild-type group with a day 3 latency to escape of 58 s for each (Fig. 6A).

Fear conditioning is an associative learning task measuring fear responses to a conditioned stimulus, in this case a cue (light and sound). In this test, the MNDU3-IDS group exhibited a fear response that was similar to wild-type controls in percent freezing during cue induction. Both the wild-type and MNDU3-IDS groups had a significantly better fear response compared with the HSCT group ($p < 0.05$). Wild-type and MNDU3-IDS groups also trended with a higher percent freezing than the MNDU3-GFP group, but this difference was not statistically significant (Fig. 6B). In conclusion, transplantation of MNDU3-IDS HSPCs into MPS II mice showed a trend toward normalization of neurobehavioral outcomes, indicating the potential for prevention of neurocognitive deficiency.

A Barnes Maze: Latency to Escape



B % Freezing Difference in Cue Test

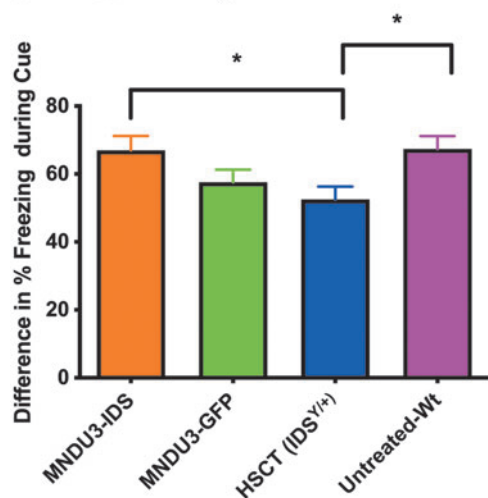


Figure 6. Neurocognitive evaluation by Barnes maze and fear conditioning cue. All four groups were evaluated neurobehaviorally at 4 months into the study. **(A)** Barnes maze as a long-term spatial memory test. Results are reported as the mean latency to escape over four trials per day for each group. Significance was assessed by two-way ANOVA. $*p < 0.05$. **(B)** Fear conditioning cue test, run as a test of learning, memory, and anxiety. Results are reported as percent difference in freezing time between the mean of three cued versus the mean of three baseline time points per mouse. Significance was determined by the Mann–Whitney U test. $*p < 0.05$. For **(A, B)**, error bars show mean \pm SD. Sample size for both tests: MNDU3-IDS $N = 12$, MNDU3-GFP $N = 11$, HSCT $N = 10$, and Untreated-Wt $N = 11$.

DISCUSSION

In this study, we evaluated *ex vivo* transduction of HSPCs using an LVV carrying a codon-optimized IDS encoding gene that is transcriptionally regulated by a constitutively active MNDU3 promoter with subsequent transplantation into MPS II mice as a potential therapeutic. Circulating IDS enzyme activity was found to be >100 times higher than wild-type levels in the plasma and in PBMCs of MNDU3-IDS transplanted mice, indicating that a high level of IDS was secreted from gene-modified hematopoietic cells and was bioavailable for cross-correction of unmodified host tissues.

Tissue analysis confirmed supraphysiological levels of IDS enzyme activity in all analyzed peripheral tissues. In the CNS, IDS activity levels were $\sim 13\%$ of wild type, sufficient to result in normalized GAG levels as observed both biochemically and histologically. Neurobehavioral evaluation showed that MNDU3-IDS-engrafted mice performed well as wild-type mice in Barnes maze and fear conditioning analyses. Finally, skeletal analysis determined that MNDU3-IDS mice had significant reduction in zygomatic arch thickness.

Initial studies of *ex vivo* LVV-transduced HSPCs for MPS II showed correction of disease in peripheral tissues, but without improvement in CNS manifestations.³⁰ Other more recent studies have evaluated the use of a tissue specific promoter, effectiveness against skeletal manifestations, and the need for a high level of engraftment.^{19–21} Here, we investigated the use of a ubiquitously expressed promoter in a comprehensive evaluation of biochemical, skeletal, histological, and neurobehavioral outcomes in MPS II mice. Circulating levels of IDS observed in our study were much higher than those reported in recent studies.^{20,21} Reasons for these differences could include transduction efficiency, overall levels of engraftment achieved, or vector design.

The sustained supraphysiological levels of circulating IDS observed in this study facilitated metabolic cross-correction of tissues, with greater than wild-type levels of IDS observed in all analyzed peripheral tissues and commensurate normalization of GAG accumulation in these tissues. Previous reports of both *ex vivo* and *in vivo* IDS gene transfer approaches have similarly shown supraphysiological levels of IDS with GAG normalization.^{17,19} We observed no toxic effect resulting from the high levels of IDS expressed in MNDU3-IDUA-treated IDS^{Y/-} mice. One concern regarding supraphysiological levels of IDS expression is the potential impact on post-translational modification and trafficking of other lysosomal hydrolases.³¹ However, recent reports have shown that elevated levels of IDS in IDS-deficient mice restore other lysosomal hydrolases to normal levels of activity.^{13,14}

As previously reported, IDS levels measured in the brains of wild-type mice were higher than any other analyzed tissues.^{15,17,19} Overall, these preclinical studies suggest that regardless of gene therapy modality, achieving wild-type levels of IDS in the mouse brain remains a significant challenge.^{15,17,19} What it is that limits IDS expression has not been reported. By comparison, MPS I preclinical gene therapy studies generally achieve higher than wild-type levels of IDUA enzyme activity in the brain.³²⁻³⁴ Conversely, preclinical gene therapy studies of MPS IIIA have also been unable to achieve wild-type levels of *N*-sulfoglucosamine sulfohydrolase.^{35,36} Although in this study normal levels of IDS in the brain were not reached, MNDU3-IDS mice achieved IDS levels in the brain that were ~13% of wild-type IDS mice and were sufficient to normalize brain GAG levels.

Previous studies have suggested that only a fraction (<5%) of wild-type IDS is needed to impact GAG accumulation in the CNS.^{15,37} Similar results have been reported in conjunction with both AAV- and LVV-based therapies for MPS II. AAV-based therapies both systemic¹⁷ and CNS directed^{14,15} have shown that increased IDS levels in the brain between 5% and 40% of wild type significantly reduced GAG content. A similar finding was reported in an *ex vivo* LVV-based study where ~5% of wild-type brain IDS activity normalized brain GAG content.¹⁹ Additionally, Laoharawee et al¹⁶ showed that as little as 1.5% of wild-type IDS reduced GAG accumulation and positively impacted neurocognitive function. Our data are consistent with these studies, as we observed normalization of brain GAGs to wild-type levels, and no significant differences were seen between MNDU3-IDS and unaffected controls in tests of spatial learning and memory in the Barnes maze as well as learning and memory in fear conditioning.

Additionally, the MNDU3-IDS group performed significantly better than the MNDU3-GFP affected control group in the Barnes maze on day 3 and the HSCT group in fear conditioning. While we observed that the MNDU3-GFP affected control mice failed to show as much of a deficit as

expected based on previous neurobehavioral analyses of similarly aged MPS II mice,^{13,15} the differences between the HSCT, MNDU3-IDS, and wild-type groups highlight the potential effectiveness of LVV gene therapy over allogeneic HSCT to impact neurological manifestations of MPS II.

The mechanism of action of allogeneic HSCT for treatment of the mucopolysaccharidoses, especially MPS I, is thought to be, in part, through donor-derived monocyte trafficking to the brain followed by differentiation into resident microglia.³⁸ These cells can then metabolically cross-correct neurons via mannose-6-phosphate receptors to reduce GAG levels and impact CNS manifestations associated with the disease.⁹ This concept also applies to autologous LVV-transduced HSPCs, whereby the progeny of transduced HSPCs traffic to the CNS, differentiate into microglia, and mediate metabolic cross-correction. To support this mechanism, we used ISH to demonstrate the presence of LVV-positive cells in the choroid plexus, perivascular regions of the brain, and in the brain meninges. However, we did not observe any LVV-positive cells in the brain parenchyma. Another possible mechanism of enzyme delivery to the brain is by circulating enzyme crossing the BBB or blood cerebrospinal fluid barrier.^{14,39}

Systemic-based studies have provided evidence that sufficiently high levels of circulating IDS enzyme can impact the CNS. A liver-directed therapy using AAV 2/8 vectors encoding zinc finger nucleases targeting the albumin locus for liver-specific expression showed a moderate level of circulating IDS, a low level of brain IDS activity, a reduction in GAG accumulation, and neurobehavioral correction.¹⁶ Similar results have been shown in studies focusing on MPS I and IDUA expression in a liver-directed strategy using intravenously administered AAV.^{39,40} However, the mechanism by which circulating enzyme accesses the CNS has not been elucidated. Given the extremely high levels of systemic IDS achieved in our study, it is thus possible that circulating IDS contributed to the observed IDS levels in the brain of MNDU3-IDS mice.

Patients with MPS II exhibit a variety of skeletal manifestations termed dysostosis multiplex. MPS II mice also display skeletal evidence of disease, such as thickening of the zygomatic arch.²² To evaluate the impact of autologous HSCT with gene-modified cells on skeletal manifestations associated with MPS II, we employed full body X-ray and Micro-CT. Wada et al²¹ recently showed that *ex vivo* gene therapy in MPS II mice can resolve bone lesions, including the zygomatic arch, by remodeling. Our skeletal analyses showed similar results in which we saw a reduction in zygomatic arch diameter, suggesting that engraftment of MNDU3-IDS-transduced cells could prevent the emergence of skeletal manifestations in MPS II mice.

Allogeneic HSCT is not considered a standard treatment option for MPS II due to the lack of evidence that it can effectively address CNS manifestations, as well as safety issues associated with allotransplant such as graft

versus host disease.^{10,41} This is in contrast to other lysosomal diseases, such as MPS I, where allogeneic HSCT is considered standard of care and there is evidence that engraftment following allogeneic HSCT can impede the onset of CNS manifestations. Given that MPS I and MPS II exhibit similar disease manifestations, why is it that only MPS I shows neurological stabilization following allogeneic HSCT?

Currently, one difference is that the time to diagnosis has been faster for MPS I than for MPS II; diagnosing and transplanting MPS II patients at an earlier age could lead to increased neurological stabilization.⁴² Indeed, some recent evidence suggests that allogeneic HSCT, particularly when administered early, could be a viable treatment option for MPS II.^{10,11} It is also possible that the amount of IDS expressed by engrafted cells may be insufficient to achieve therapeutic effectiveness. If this is the case, *ex vivo* gene transfer may be a better option for delivering more gene-modified cells capable of producing supraphysiological levels of enzyme compared with allogeneic HSCT.

In this study, we report that MPS II mice engrafted with MNDU3-IDS-transduced HSPCs exhibit supraphysiological levels of circulating, bioavailable IDS enzyme capable of tissue cross-correction as evidenced by normalization of GAGs. In the CNS, increased levels of IDS activity with concurrent GAG normalization was observed as well as a benefit to neurocognitive function. Overall, this study supports the potential therapeutic efficacy of *ex vivo* MNDU3-IDS LVV-transduced HSPCs for MPS II patients.

ACKNOWLEDGMENTS

We thank Mouse Behavior Core directors Dr. Bennyworth and Dr. Larson for help with testing. We thank Amelia Thomas for preparing the vector and Gina Scarglia for her contribution on tissue processing, histochemical, and immunohistochemical staining. We thank Dr. Joseph Muenzer for providing the IDS-KO mouse strain. This study was previously presented as a poster at *WORLDsymposium* including a published abstract from the conference proceedings. We thank Brenda Koniar for assisting in the bone marrow transplants.

AUTHORS' CONTRIBUTIONS

M.C.S.: experimental design and overall coordination, HSPC transduction and transplants, flow cytometry, tissue collection and processing, IDS enzyme and GAG assays, neurobehavioral testing, compiling all results, and lead role in article writing. L.R.B.: study design, data interpretation, and article writing. A.D.K. and K.M.P.-P.: HSC transplants and in-life collections. O.E.: GAG assays. J.M.: study coordination, vector characterization, and validation. J.D.: vector characterization and validation. K.G.: study design, data interpretation, and article writing. G.P.: vector design, study design and coordination, data interpretation, and article writing. N.R.: histopathological analysis and article writing. S.L.: study design, gross tissue evaluation, and histochemical and immunohistochemical staining. S.S.: VCN analysis, study coordination, data interpretation, and article writing. J.F. and T.C.L.: X-ray and micro-CT radiography, and analysis. H.-C.T., R.S.M., and M.B.: study design and coordination, data interpretation, and article writing.

AUTHOR DISCLOSURE

The work detailed in this article was sponsored by bluebird bio, Inc. J.M., J.D., K.G., G.P., N.R., S.L., S.S., H.-C.T., and M.B. are all current or former employees of bluebird bio, Inc. The remaining authors declare no competing interests.

FUNDING INFORMATION

Neurobehavioral studies were performed in the Mouse Behavior Core at the University of Minnesota (supported by the National Institutes of Health grant NS062158). M.C.S. was supported by grant number: 5T32GM113846-10 Stem Cell Biology Training Program T32 at the University of Minnesota. This project was supported by bluebird bio through a Sponsored Research Agreement with the University of Minnesota.

SUPPLEMENTARY MATERIAL

Supplementary Figure S1

Supplementary Figure S2

REFERENCES

- Hampe CS, Yund BD, Orchard PJ, et al. Differences in MPS I and MPS II disease manifestations. *Int J Mol Sci* 2021;22(15):7888; doi: 10.3390/ijms22157888
- Zapolnik P, Pyrkosz A. Gene therapy for mucopolysaccharidosis type II—A review of the current possibilities. *Int J Mol Sci* 2021;22(11):5490; doi: 10.3390/ijms22115490
- Neufeld EF, Muenzer J. The Mucopolysaccharidoses. In: *The Online Metabolic and Molecular Bases of Inherited Disease*. (Valle DL, Antonarakis S, Ballabio A, et al. eds.) McGraw-Hill Education: New York, NY, 2019; pp. 3421–3452.
- Kim C, Seo J, Chung Y, et al. Comparative study of idursulfase beta and idursulfase in vitro and in vivo. *J Hum Genet* 2017;62(2):167–174; doi: 10.1038/jhg.2016.133
- Sohn YB, Cho SY, Park SW, et al. Phase I/II clinical trial of enzyme replacement therapy with idursulfase beta in patients with mucopolysaccharidosis II (Hunter syndrome). *Orphanet J Rare Dis* 2013;8:42; doi: 10.1186/1750-1172-8-42
- Parini R, Rigoldi M, Tedesco L, et al. Enzymatic replacement therapy for Hunter disease: Up to 9 years experience with 17 patients. *Mol Genet Metab Rep* 2015;3:65–74; doi: 10.1016/j.ymgmr.2015.03.011
- D'Avanzo F, Rigon L, Zanetti A, et al. Mucopolysaccharidosis type II: One hundred years of

- research, diagnosis, and treatment. *Int J Mol Sci* 2020;21(4):1258; doi: 10.3390/ijms21041258
8. Lagler FB. Current and Emerging Therapies for Mucopolysaccharidoses. In: *Pediatric Pharmacotherapy*. (Kiess W, Schwab M, van den Anker J. eds.) Handbook of Experimental Pharmacology Springer International Publishing: Cham, 2020; pp. 39–56.
 9. Biffi A. Hematopoietic stem cell gene therapy for storage disease: Current and new indications. *Mol Ther* 2017;25(5):1155–1162; doi: 10.1016/j.ymthe.2017.03.025
 10. Selvanathan A, Ellaway C, Wilson C, et al. Effectiveness of early hematopoietic stem cell transplantation in preventing neurocognitive decline in mucopolysaccharidosis type II: A case series. *JIMD Rep* 2018;41:81–89; doi: 10.1007/8904_2018_104
 11. Kubaski F, Yabe H, Suzuki Y, et al. Hematopoietic stem cell transplantation for patients with mucopolysaccharidosis II. *Biol Blood Marrow Transplant* 2017;23(10):1795–1803; doi: 10.1016/j.bbmt.2017.06.020
 12. Biffi A. Gene therapy for lysosomal storage disorders: A good start. *Hum Mol Genet* 2016;25(R1):R65–R75; doi: 10.1093/hmg/ddv457
 13. Hinderer C, Katz N, Louboutin J-P, et al. Delivery of an adeno-associated virus vector into cerebrospinal fluid attenuates central nervous system disease in mucopolysaccharidosis type II mice. *Hum Gene Ther* 2016;27(11):906–915; doi: 10.1089/hum.2016.101
 14. Motas S, Haurigot V, Garcia M, et al. CNS-directed gene therapy for the treatment of neurologic and somatic mucopolysaccharidosis type II (Hunter syndrome). *JCI Insight* 2016;1(9):e86696; doi: 10.1172/jci.insight.86696
 15. Laoharawee K, Podetz-Pedersen KM, Nguyen TT, et al. Prevention of neurocognitive deficiency in mucopolysaccharidosis type II mice by central nervous system-directed, AAV9-mediated iduronate sulfatase gene transfer. *Hum Gene Ther* 2017;28(8):626–638; doi: 10.1089/hum.2016.184
 16. Laoharawee K, DeKelver RC, Podetz-Pedersen KM, et al. Dose-dependent prevention of metabolic and neurologic disease in murine MPS II by ZFN-mediated in vivo genome editing. *Mol Ther* 2018;26(4):1127–1136; doi: 10.1016/j.ymthe.2018.03.002
 17. Fu H, Zaraspe K, Murakami N, et al. Targeting root cause by systemic scAAV9-hIDS gene delivery: Functional correction and reversal of severe MPS II in mice. *Mol Ther Methods Clin Dev* 2018;10:327–340; doi: 10.1016/j.omtm.2018.07.005
 18. Mingozzi F, High KA. Immune responses to AAV vectors: Overcoming barriers to successful gene therapy. *Blood* 2013;122(1):23–36; doi: 10.1182/blood-2013-01-306647
 19. Gleitz HF, Liao AY, Cook JR, et al. Brain-targeted stem cell gene therapy corrects mucopolysaccharidosis type II via multiple mechanisms. *EMBO Mol Med* 2018;10(7):e8730; doi: 10.15252/emmm.201708730
 20. Miwa S, Watabe AM, Shimada Y, et al. Efficient engraftment of genetically modified cells is necessary to ameliorate central nervous system involvement of murine model of mucopolysaccharidosis type II by hematopoietic stem cell targeted gene therapy. *Mol Genet Metab* 2020;130(4):262–273; doi: 10.1016/j.ymgme.2020.06.007
 21. Wada M, Shimada Y, Iizuka S, et al. Ex vivo gene therapy treats bone complications of mucopolysaccharidosis type II mouse models through bone remodeling reactivation. *Mol Ther Methods Clin Dev* 2020;19:261–274; doi: 10.1016/j.omtm.2020.09.012
 22. Garcia AR, Pan J, Lamsa JC, et al. The characterization of a murine model of mucopolysaccharidosis II (Hunter syndrome). *J Inher Metab Dis* 2007;30(6):924–934; doi: 10.1007/s10545-007-0641-8
 23. Friedman KM, Garrett TE, Evans JW, et al. Effective targeting of multiple B-cell maturation antigen-expressing hematological malignancies by anti-B-cell maturation antigen chimeric antigen receptor T cells. *Hum Gene Ther* 2018;29(5):585–601; doi: 10.1089/hum.2018.001
 24. Forte G, Minieri M, Cossa P, et al. Hepatocyte growth factor effects on mesenchymal stem cells: Proliferation, migration, and differentiation. *Stem Cells* 2006;24(1):23–33; doi: 10.1634/stemcells.2004-0176
 25. Heffner GC, Bonner M, Christiansen L, et al. Prostaglandin E2 increases lentiviral vector transduction efficiency of adult human hematopoietic stem and progenitor cells. *Mol Ther* 2018;26(1):320–328; doi: 10.1016/j.ymthe.2017.09.025
 26. Xu L, Mango RL, Sands MS, et al. Evaluation of pathological manifestations of disease in mucopolysaccharidosis VII mice after neonatal hepatic gene therapy. *Mol Ther* 2002;6(6):745–758; doi: 10.1006/mthe.2002.0809
 27. Pitts MW. Barnes maze procedure for spatial learning and memory in mice. *Bio Protoc* 2018;8(5):e2744; doi: 10.21769/bioprotoc.2744
 28. Shoji H, Takao K, Hattori S, et al. Contextual and cued fear conditioning test using a video analyzing system in mice. *J Vis Exp* 2014;(85):50871; doi: 10.3791/50871
 29. Rigon L, Kucharowski N, Eckardt F, et al. Modeling mucopolysaccharidosis type II in the fruit fly by using the RNA interference approach. *Life (Basel)* 2020;10(11):263; doi: 10.3390/life10110263
 30. Wakabayashi T, Shimada Y, Akiyama K, et al. Hematopoietic stem cell gene therapy corrects neuropathic phenotype in murine model of mucopolysaccharidosis type II. *Hum Gene Ther* 2015;26(6):357–366; doi: 10.1089/hum.2014.158
 31. Anson DS, Bielicki J, Hopwood JJ. Correction of mucopolysaccharidosis type I fibroblasts by retroviral-mediated transfer of the human α -L-iduronidase gene. *Hum Gene Ther* 1992;3(4):371–379; doi: 10.1089/hum.1992.3.4-371
 32. Wolf DA, Lenander AW, Nan Z, et al. Direct gene transfer to the CNS prevents emergence of neurologic disease in a murine model of mucopolysaccharidosis type I. *Neurobiol Dis* 2011;43(1):123–133; doi: 10.1016/j.nbd.2011.02.015
 33. Visigalli I, Delai S, Politi LS, et al. Gene therapy augments the efficacy of hematopoietic cell transplantation and fully corrects mucopolysaccharidosis type I phenotype in the mouse model. *Blood* 2010;116(24):5130–5139; doi: 10.1182/blood-2010-04-278234
 34. Belur LR, Romero M, Lee J, et al. Comparative effectiveness of intracerebroventricular, intrathecal, and intranasal routes of AAV9 vector administration for genetic therapy of neurologic disease in murine mucopolysaccharidosis type I. *Front Mol Neurosci* 2021;14:618360; doi: 10.3389/fnmol.2021.618360
 35. Bobo TA, Samowitz PN, Robinson MI, et al. Targeting the root cause of mucopolysaccharidosis IIIA with a new scAAV9 gene replacement vector. *Mol Ther Methods Clin Dev* 2020;19:474–485; doi: 10.1016/j.omtm.2020.10.014
 36. Sergijenko A, Langford-Smith A, Liao AY, et al. Myeloid/microglial driven autologous hematopoietic stem cell gene therapy corrects a neuronopathic lysosomal disease. *Mol Ther* 2013;21(10):1938–1949; doi: 10.1038/mt.2013.141
 37. Polito VA, Cosma MP. IDS crossing of the blood-brain barrier corrects CNS defects in MPSII mice. *Am J Hum Genet* 2009;85(2):296–301; doi: 10.1016/j.ajhg.2009.07.011
 38. Capotondo A, Milazzo R, Politi LS, et al. Brain conditioning is instrumental for successful microglia reconstitution following hematopoietic stem cell transplantation. *Proc Natl Acad Sci U S A* 2012;109(37):15018–15023; doi: 10.1073/pnas.1205858109
 39. Belur LR, Podetz-Pedersen KM, Tran TA, et al. Intravenous delivery for treatment of mucopolysaccharidosis type I: A comparison of AAV serotypes 9 and rh10. *Mol Genet Metab Rep* 2020;24:100604; doi: 10.1016/j.ymgmr.2020.100604
 40. Ou L, DeKelver RC, Rohde M, et al. ZFN-mediated in vivo genome editing corrects murine Hurler syndrome. *Mol Ther* 2019;27(1):178–187; doi: 10.1016/j.ymthe.2018.10.018
 41. Taylor M, Khan S, Stapleton M, et al. Hematopoietic stem cell transplantation for mucopolysaccharidoses: Past, present, and future. *Biol Blood Marrow Transplant* 2019;25(7):e226–e246; doi: 10.1016/j.bbmt.2019.02.012
 42. Nan H, Park C, Maeng S. Mucopolysaccharidoses I and II: Brief review of therapeutic options and supportive/palliative therapies. *Biomed Res Int* 2020;2020:2408402; doi: 10.1155/2020/2408402
 43. Challita PM, Skelton D, el-Khoueiry A, et al. Multiple modifications in cis elements of the long terminal repeat of retroviral vectors lead to increased expression and decreased DNA methylation in embryonic carcinoma cells. *J Virol* 1995;69(2):748–755.

Received for publication June 30, 2022;
accepted after revision September 2, 2022.

Published online: October 13, 2022.